We are IntechOpen,
the world's leading publisher of
Open Access books
Built by scientists, for scientists

6,900
Open access books available

186,000
International authors and editors

200M
Downloads

Our authors are among the

154
Countries delivered to

TOP 1%
most cited scientists

12.2%
Contributors from top 500 universities

CLARIVATE ANALYTICS
BOOK CITATION INDEX
INDEXED

WEB OF SCIENCE™

Selection of our books indexed in the Book Citation Index
in Web of Science™ Core Collection (BKCI)

Interested in publishing with us?
Contact book.department@intechopen.com

Co-Ionic Conduction in Protonic Ceramics of the Solid Solution, $BaCe_{(x)}Zr_{(y-x)}Y_{(1-y)}O_{3-\delta}$ Part I: Fabrication and Microstructure

W. Grover Coors
CoorsTek, Inc.
USA

1. Intoduction

Protonic ceramics have unique transport properties that make them suitable for applications in intermediate temperature fuel cells and steam electrolyzers, hydrogen separation membranes, and various membrane reactors for chemical synthesis. Since the discovery of ceramic proton conductors more than twenty years ago, and the ensuing enthusiasm, practical issues relating to ceramic fabrication have hampered advancement of the technology. The best ceramic proton conductors were thought to be acceptor-doped barium cerates, but these turned out not to be chemically stable in the typical use environments. The other leading candidates, acceptor-doped barium zirconates, proved too difficult to sinter. Most other protonic ceramics investigated either exhibited much lower conductivity or poor chemical stability. Two breakthroughs have recently taken place making it feasible, for the first time, to manufacture these ceramic proton conductors commercially and inexpensively with the prerequisite properties. First, the recognition that barium cerate and barium zirconate form a complete solid solution ($BaCe_xZr_{y-x}Y_{1-y}O_{3-\square}$, for all values of $1 > y > 0.8$ and x between 0 and y), has made it possible to tailor the mechanical, chemical and transport properties for various applications. Second, the discovery of solid state reactive sintering has made it possible to prepare dense, phase-pure ceramics at reasonable temperatures. This chapter describes fabrication and characterization of BCZY proton conductors using 1-2 wt% NiO as a sintering additive for solid state reactive sintering.

2. Background

Certain ABO_3 perovskite ceramic oxides containing acceptor dopants have high concentrations of extrinsic oxygen ion vacancies that give rise to unique ionic transport properties. Many ceramic proton conductors in this group have been identified, most notably where A = Ba or Sr and B = Ce or Zr. Certain aliovalent cations, where Y^{+3} is prototypical, may substitute for B sites otherwise occupied by Ce^{+4} or Zr^{+4}, in mole fractions as high as 20-30% before the structure becomes unstable. The resulting charge imbalance in the crystal lattice is compensated for by the creation of oxygen ion vacancies on the anion sublattice. These oxygen ion vacancies each carry a net double-positive charge, so that two dopant ions are required for each oxygen ion vacancy created, in order to maintain

electroneutrality. Yttrium-doped barium cerate, $BaCe_{(1-x)}Y_xO_{3-d}$ (BCY), has long been recognized as one of the best ceramic proton conductors. Iwahara carried out the first systematic evaluation of the ionic conduction properties of barium cerate in 1988 (Iwahara, et al., 1988). It is straightforward to fabricate this ceramic material by traditional solid-state reaction, and for this reason, it has been one of the most extensively studied of all the ceramic proton conductors. Nonetheless, concerns have persisted about the chemical stability in moist carbon dioxide, which corrodes the ceramic to form barium carbonate and hydroxide. Since many applications for ceramic proton conductors involve operation in hot, moist CO and CO_2 atmosphere, interest in BCY as a practical material has waned.

Yttrium-doped barium zirconate, $BaZr_{(1-x)}Y_xO_{3-d}$ (BZY) has also been recognized as a good ceramic proton conductor for many years, but without the same concerns about chemical stability in moist CO_2 as with BCY. Kreuer reported transport properties of BZY for the first time using single crystals and sintered ceramics (Kreuer, 1999). Schober and Bohn were also able to prepare dense ceramic specimens (Schober & Bohn, 2000), although as was the case with Kreuer, a sintering temperature above 1700 °C for 30 hours was required. Difficulty in producing dense polycrystalline specimens has hindered the development of this material. The traditional processing routes of synthesizing fine powders by solid-state reaction or spray pyrolysis produce powders that are difficult to sinter below 1700 °C, even when hot-pressed. The reason that the material is so difficult to sinter is not yet fully understood, but firing at such high temperatures tends to volatilize barium, leaving the material A-site deficient, and the resulting ceramic exhibits poor proton conductivity. Magrez and Schober successfully synthesized dense BZY at 1500 °C by a polyacrilamide gel method (Magrez & Schober, 2004), but the method has apparently never been fully optimized. Münch published a comparative analysis of BCY and BZY by quantum molecular dynamics simulation (Münch, et al., 2000), which suggested that BZY should be, in principle, a very good proton conductor. However, high impedance to proton transport across grain boundaries in polycrystalline specimens is thought to be the main reason that measured ionic conductivity is much lower than predicted. More recently, many interesting methods have been proposed for synthesizing polycrystalline BZY. Perhaps one of the most ingenious involves converting a thin layer of 8 mol% yttria-stabilized zirconia (8YSZ) into BZY by reacting with $BaCO_3$ in situ (Schober, 2005). Nonetheless, to our knowledge, the high grain boundary impedance problem has never been solved using traditional synthesis, dampening commercial interest in pure BZY as a proton conductor. A comprehensive review of the progress on these materials prior to 2003 has been provided by Kreuer (Kreuer, 2003).

A critical breakthrough in producing BZY was first reported by Babilo and Haile, who found that dense BZY ceramics could be prepared at a sintering temperature of only 1300 °C for four hours when transition metal oxides, ZnO, CuO or NiO, were added up to 4 mol% (Babilo & Haile, 2005). Without the addition, BZY remained substantially porous. Independently, Tao and Irvine demonstrated the same discovery of ZnO as an effective sintering additive for preparing BZY (Tao & Irvine, 2006, 2007). The effect has subsequently been reported by several investigators (Tong, et al., 2010a, 2010b; Wang, et al., 2009; Xu, et al., 2010). Enhanced sinterability of BZY with 1 wt% NiO has been demonstrated in our lab (Coors, 2008). The exact mechanism responsible for the dramatic improvement in sinterability remains controversial, but the result has been widely confirmed. Transition

metal oxides have also been used as sintering aids with BCY to lower the sintering temperature and to investigate the effect of these additions on conductivity. Shimura used Mn, Co and Fe - finding cobalt to be the most effective (Shimura, et al., 2005). Costa reported that 4 mol% NiO lowered the sintering temperature of BCY by 200 °C (Costa, et al., 2009). Tong used 2 mol% NiO to fabricate BCY20 (Tong, et al. 2010c), and we also confirmed this effect with NiO in our lab (Coors, et al., 2009). In all cases, no significant difference in conductivity of BCY has been observed, with or without these sintering aids, so it has generally been concluded that small additions of 2+ transition metal oxides has negligible impact on the transport properties and structure, other than to enhance sintering and increase average grain size. In the case of BZY20, Tong and O'Hayre reported high conductivities in moist argon (Tong, et al., 2010a, 2010b). A clear path forward to producing these protonic ceramic materials now seems possible.

In the meantime, a parallel path in the development of ceramic proton conductors was being pursued. The idea of solid solutions of BCY and BZY was initially proposed by Wienströer & Wiemhöfer stating that, "A solid proton conductor that combines the higher chemical stability of the zirconates and the high conductivity of the cerates could solve these problems" (Wienströer & Wiemhöfer, 1997). Since barium cerate and barium zirconate are nearly isomorphic, it was expected that they would be end members of a binary solid solution where B-sites are randomly occupied by either Zr^{+4} or Ce^{+4}. This idea was demonstrated for BaCe$_{0.9-x}$Zr$_x$Nd$_{0.1}$O$_{2.95}$ for 0.1≤x≤0.6 by Ryu (Ryu & Haile, 1999) and subsequently for BaCe$_{0.9-x}$Zr$_x$Gd$_{0.1}$O$_{2.95}$ for 0<x<0.4. Katahira (Katahira, et al. 2000), Zhong (Zhong, 2007), Ricote (Ricote, et al., 2009a, 2009b) and Guo (Guo, et al. 2009) extended the investigation to yttria dopant in BaCe$_{0.9-x}$Zr$_x$Y$_{0.1}$O$_{2.95}$ for 0≤x≤0.9. These papers all confirmed that a stable solid solution existed, and that chemical stability could be improved without significantly diminishing the protonic conductivity. However, it still proved difficult in practice to obtain uniform mixing of the BCY and BZY phases, and high sintering temperatures were still required to prepare dense polycrystalline specimens.

The solution to this problem was, naturally, to extend the use of transition metal oxide sintering additives, originally used only with the end members, BCY and BZY, to the whole range of solid solutions. This approach was first reported by Tao (Tao & Irvine, 2007) and more recently by Wang (Wang, et al., 2009). Azimova reported BCZY using CoO as a sintering aid (Azimova & McIntosh, 2009). Most recently Ricote reported very satisfactory results for BaCe$_{0.2}$Zr$_{0.7}$Y$_{0.1}$O$_{2.95}$ prepared by solid state reactive sintering using 1-2 wt% NiO (Ricote, et al., 2011). The development of protonic ceramics based on BCY-BZY solid solutions with transition metal oxide sintering aids has provided new latitude in the design of functional proton conductors and has now become a significant factor in the development of practical protonic ceramics.

2.1 Nomenclature

A note on nomenclature is in order. The number of compositional variants of these materials is enormous. In order to avoid writing out the entire formula each time, abbreviations are typically used, but almost every investigator has a unique system, and there has been no consistency in the literature. Also, BaCe$_x$Zr$_{0.9-x}$Y$_{0.1}$O$_{2.95}$ often appears as BaCe$_{0.9-x}$Zr$_x$Y$_{0.1}$O$_{2.95}$ – the only difference being which B-site cation the variable applies to. Ricote and colleagues at Risø in Denmark recently proposed a simple notation that solves these problems, and will be used throughout the following text (Ricote, et al., 2009). The basic formula is BCZM*nm*,

for barium, cerium, zirconium and M-dopant (Y, Gd, Nd, etc.). The cerium and zirconium mole fractions are n and m times ten. The nominal B-site occupancy is $x_M + x_n + x_m = 1$. The critical ratio n/m can be correlated to chemical stability. The dopant mole fraction x_M is implied as $(1 - x_m - x_n)$. For example, $BaCe_{0.5}Zr_{0.4}Y_{0.1}O_{3-d}$ becomes BCZY54, and BCZY44 refers to $BaCe_{0.4}Zr_{0.4}Y_{0.2}O_{2.95}$. The end members of the solid solution, which were previously often designated as BCY20 and BZY20, now become BCZY80 and BCZY08, respectively, in the new nomenclature. A complication with this notation arises when sintering aids or secondary dopants are used. The Risø notation cannot easily accommodate multiple B-site dopants. Nonetheless, without some type of simplifying notation, the formulas become needlessly complex and difficult to compare. In what follows, only the major dopant will be included in the formula with the sintering additive given as a prefix, for example, 2NiBCZY26 is just $BaCe_{0.2}Zr_{0.6}Y_{0.2}O_{2.95}$ plus 2 wt% NiO.
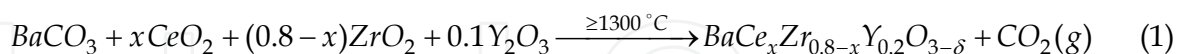
For hydrogen/air protonic ceramic fuel cells PCFCs and steam electrolysis cells PCECs (Irvine, et al. 2007), where humid air is used, chemical stability against CO_2 below about 1% may be sufficient. But the most interesting applications for protonic ceramics that are now being considered will require stability against much higher concentrations. For example, the anode gas of a PCFC operating on methane or other hydrocarbon fuels at high fuel utilization will approach 100% CO_2. Various electrolytic cells for producing syngas, including membrane reactors, may also be expected to have high CO and CO_2 concentrations in contact with the ceramic at moderate temperatures ranging from 500 to 800 °C. The end member, barium cerate (BCZY90), is unstable in CO_2, but several investigations have been carried out to determine the maximum value of the ratio of Ce/Zr (n/m) for which the ceramic is chemically stable. Tao reported ZnO-BCZY53 to be stable in pure CO_2 in this range of temperatures (Tao & Irvine, 2006). Ryu reported that the more ceria-rich, ZnO-BCZY72 is also stable in CO_2 for the ratio of $n/m \leq 7/2$ (Ryu & Haile, 1999). However, Zhong observed a small amount of $BaCO_3$ formation at BCZY72, but not in BCZY54 (Zhong, 2007). Ricote similarly found BCZY63 to be unstable, while BCZY27 was completely stable in pure CO_2 (Ricote, et al., 2009).

3. Reactive sintering

It is a good idea from the outset to carefully lay down definitions for the term, *reactive sintering*, and the other related terms that have to do with how polycrystalline ceramic materials are actually fabricated from powders. The idea of reactive sintering is nothing new. Kingery described it in his definitive textbook on ceramics, "During the firing process…in many ceramics there may be solid-state reactions forming new phases, polymorphic transformations, [and] decompositions of crystalline compounds to form new phases …" (Kingery 1960, p.448). Reactive sintering is an important industrial process, but it is often overlooked during the research and development phase because of the convenience of procuring high purity pre-calcined ceramic powders.

Solid-state reaction: Solid state-reaction is a general term that pertains (in the context of making ceramics) to producing new solid product phases from other reactant phases below the melting point of either products or reactants. At a given temperature, the phase with the lowest Gibbs free energy will prevail, but because ion mobility in solids is often very low, even near the melting point, equilibrium may not be achieved in reasonable time scales. Solid-state reactions require intermixing of ions from reactant phases by solid state diffusion, therefore, solid-state reactions are enhanced by making the diffusion lengths as

Co-Ionic Conduction in Protonic Ceramics of the
Solid Solution, $BaCe_{(x)}Zr_{(y-x)}Y_{(1-y)}O_{3-\delta}$ Part I: Fabrication and Microstructure
483

short as possible. This is commonly accomplished by starting with very fine, well-mixed reactant crystallites that can be obtained by attrition milling, sol-gel methods or pyrolysis of salts precipitated from solution. Almost all specialty ceramic powders are prepared by one of these techniques. One common method for making fine, single phase BCZY powder is by solid-state reaction using carbonates and oxides.

$$BaCO_3 + xCeO_2 + (0.8 - x)ZrO_2 + 0.1Y_2O_3 \xrightarrow{\geq 1300\,^\circ C} BaCe_xZr_{0.8-x}Y_{0.2}O_{3-\delta} + CO_2(g) \qquad (1)$$

Traditional sintering: The traditional approach to fabricating ceramic perovskites is to begin by preparing phase pure powders of the correct stoichiometry by solid-state reaction (such as Eq.1), milling the resulting powder, called *calcine*, and then compacting the powder into green bodies for subsequent ceramic sintering at high temperatures.

Solid-State Reactive Sintering: For solid-state reactive sintering, SSRS, the discrete steps of solid-state reaction and traditional powder sintering are combined into a single processing step. The precursor powders are mixed with binders and compacted into a green body. This is only possible when the kinetics of solid state reaction are fast enough so that reaction-product crystallites form prior to, or simultaneously with, sintering. This fabrication method has been described by Babilo and Haile, where certain transition metal oxides, such as NiO, ZnO, and CuO, were included in the formulation (Babilo & Haile, 2005), and Tao with ZnO (Tao & Irvine, 2006). The transition metal oxides promote the formation of the equilibrium phase while simultaneously enhancing densification by sintering.

Sintering additives: The metal oxide is more than just a "sintering aid". A traditional sintering aid promotes transport at the surface along grain boundaries, assisting densification, without substantially interacting with the bulk phases. In reactive sintering, the metal oxide ions are believed to play a crucial role in ion exchange and diffusion within the grains as well as at grain boundaries. Often a eutectic liquid phase forms between the transition metal oxide and the alkali metal, dissolving the other oxides, from which the desired perovskite phase is produced. In this sense, transition metal oxides are used as reactive sintering *additives*. The solubility limit of NiO in the host BCZY is about 1 wt%. Any additional NiO shows up as a distinct second phase. There is some controversy surrounding where the dissolved nickel ions end up after sintering – whether they go into interstitial sites or substitute for B- or even A-sites, or remain at grain boundaries as an amorphous second phase. These questions may have considerable bearing on the electronic properties, but as a practical matter, it is nearly impossible to draw any concrete conclusions about nickel in the structure at such low concentrations.

In a recent development, Yamazaki reported that dense BZY ceramics could be prepared at moderate sintering temperature by SSRS without any sintering additives at all (Yamazaki, et al., 2009). That is, the solid-state reaction and sintering steps were carried out simultaneously, but apparently without the need for sintering additives (beyond the trace impurities in the starting materials). This raises new questions about what role played by transition metal oxides in the sintering process, possibly opening up a whole new direction in practical protonic ceramic fabrication. In our lab, we have found that when a slurry of precursor oxides and carbonates is applied to the surface of a NiO-BCZY composite substrate, a thin film membrane of dense BCZY electrolyte forms during co-sintering, even when no NiO is added to the slurry. During sintering, some NiO diffuses from the substrate into the membrane up to the solubility limit of about 1 mol%, but whether or not this NiO is actually necessary for densification of the membrane is not known at this time. A polished

section of a supported membrane produced this way is shown in Figure 1. The light areas are BCZY26 phase and the grey areas are NiO grains. (The dark region on the left is potting compound.) A dip coated and co-fired BCZY26 electrolyte membrane, about 15 µm thick, and typical of the membranes required for various practical devices, is shown. It is apparent from the image that both phases are independently contiguous except through the membrane region, which shows no evidence of penetration by NiO. It is also apparent in the image that the sintered specimen is almost fully dense. The residual spherical pores visible within the NiO grains are typical of liquid phases formed during sintering. No porosity is visible in the BCZY26 phase or at BCZY26/NiO grain boundaries.
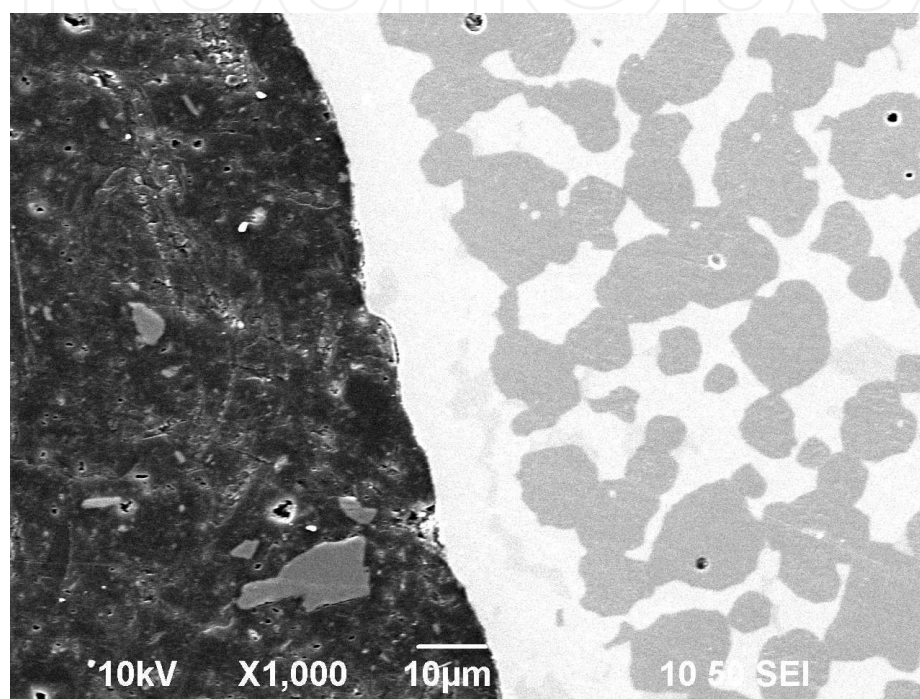

Fig. 1. Polished cross section of as-fired (unreduced) 68NiBCZY26 with 15 µm dip-coated membrane. Light regions are BCZY26 and dark regions are NiO (SEI-1000x).

4. Ceramic fabrication method

Precursor powders, $BaCO_3$, CeO_2, ZrO_2 and Y_2O_3 were dried and weighed to obtain the desired nominal stoichiometery for the $BaCe_xZr_{0.8-x}Y_{0.2}O_{2.9}$. An additional 1 wt% NiO was included as a sintering additive, but was not included in the stoichiometry, as we have found that NiO resides at grain boundaries, and nickel ions do not remain in the ABO_3 perovskite structure after sintering. Specimens of 1NiBCZY, with 20 mol% Y and Ce-Zr; 80, 44, 26, and 08, and 10 mol% Y with Ce-Zr; 45, 36, 27, 18, 09 were prepared for XRD analysis by conventional powder processing in a 19mm diameter uniaxial compaction die. Extruded 1NiBCZY26 and 1NiBCZY27 tubes were also fabricated by solid state reactive sintering from precursor oxides and carbonates. Barium carbonate (Alfa Aesar, tech grade, 99.6%, Item# 43478, $BaCO_3$), zirconium oxide (Neo Performance Materials (AMR Ltd), ≥99.5%, Item# 2802004, ZrO_2), cerium oxide (Neo Performance Materials (AMR Ltd), ≥99.5%, Item# 4-02-13-01, CeO_2), yttrium oxide (HJD Intl. 99.99+%, ultra fine, Y_2O_3) and nickel oxide (Inco, Grade F NiO) were used for the synthesis of the ceramic tubes, prepared according to the

Co-Ionic Conduction in Protonic Ceramics of the
Solid Solution,$BaCe_{(x)}Zr_{(y-x)}Y_{(1-y)}O_{3-\delta}$ Part I: Fabrication and Microstructure
485

powder formulation given in Table 1 for BCZY26, as an example. The precursor powders were blended with water soluble acrylic and cellulosic ether plasticizers. The tubes were extruded on a 40-ton Loomis extruder. The spindle diameter was 7.14 mm and die diameter was 9.91mm. The extruded tubes were dried for a week in controlled humidity on plaster V-groove setters. The dried tubes were hang-fired on zirconia pins extending through one end. The length of the green tubes was 46 cm. The tubes were sintered at 1500 °C for 4 hours in air at a heating rate is 50 °C/hr up to 450 °C and 100 °C/hr up to 1500 °C. All specimens were greater than 98% dense as determined by Archimedes method.

Material	Form.wt.	Mole/FU	Wt./FU	Wt.fract.
$BaCO_3$	197.35	1.0	197.35	0.595
CeO_2	172.12	0.2	34.42	0.104
ZrO_2	123.22	0.6	73.93	0.223
Y_2O_3	225.81	0.1	22.58	0.068
$NiO(1w\%)$	74.71	-	-	0.010
		total	328.28	1.000

Table 1. Powder formulation for 1NiBCZY26 (based on $BaCe_{0.2}Zr_{0.6}Y_{0.2}O_{3-d}$, form.wt. = 284.263 g/mol)

The stoichiometry of the sintered BCZY26 tubes was confirmed by X-ray Fluorescence using fused samples and standards in lithium tetraborate glass on a PANalytical MagiX Model 2440, sequential 3.0 kW XRF. The results are given in Table 2, which shows weight percent based on oxides and calculated mol%. A significant fraction of strontia was found to coexist with baria. Also, some alumina and a trace of iron oxide were detected. The site fractions were calculated assuming pure ABO_3 perovskite with Ba and Sr only on A-sites and Ce, Zr and Y on B-sites, giving the nominal stoichiometry: $Ba(Sr)_{1.002}Ce_{0.202}Zr_{0.586}Y_{0.198}O_{2.90}$. B-site occupancy sums to 1.004, giving an error less than 1%. Thus, a small amount of B-site Ni ions (Ni^{+2} or Ni^{+3}) cannot be ruled out, but the net effect is negligible.

Material	Wt%	Form.wt.	Mol/100g	Mol.fract
BaO	51.70	153.326	0.3372	0.959
SrO	1.59	103.619	0.0153	0.043
CeO_2	12.20	123.223	0.0709	0.202
ZrO_2	25.40	172.115	0.2061	0.586
Y_2O_3	7.88	225.81	0.0349	0.198
			total	1.988
NiO	1.05	74.693	0.0141	
Al_2O_3	0.22	101.961	0.0022	
Fe_2O_3	<0.01			

Table 2. XRF analysis of 1NiBCZY26 based on formula wt. = 284.263 g/mol

XRD was performed using an X'Pert XRD diffractometer from 10 to 90 degrees with 0.02 degree increments. SEM analysis was performed on a JOEL JSM-6390 and field emission FESEM was performed on a JEOL JSM-7000F with an energy dispersive spectroscopy detector (EDS) from EDAX. Imaging was conducted using a 2 kV electron beam and EDS was obtained using a 5 kW electron beam. Bright field TEM was performed on FIB-prepared

specimens. Magnetic characterization measurements on a reduced specimen was performed on a Quantum Design PPMS equipped with the VSM and oven options. The relative amounts of metallic nickel and residual nickel ions were measured at 2K against a pure nickel wire scaled to the same 1 wt% NiBCZY26 specimen.

5. Phase and microstructure

5.1 XRD

The XRD patterns for dense ceramic specimens of BCZY prepared by reactive sintering with 1 wt% NiO addition are shown in Figure 2. The four specimens span the entire composition range from pure BZY (BCZY08) to BCY (BCZY80). The major perovskite peaks are shown indexed to the cubic system of $BaZrO_3$ (74-1299). $BaCeO_3$ (83-0532) is orthorhombic, so the index is pseudocubic in this case (45° rotation with respect to the cubic lattice parameter

$$\bar{a} = \left(\frac{a}{\sqrt{2}} + \frac{b}{\sqrt{2}} + \frac{c}{2} \right) / 3 \text{).}$$ The dominant feature of the XRD patterns is the uniform

decrease in lattice parameter in going from BCZY80 to BCZY08.
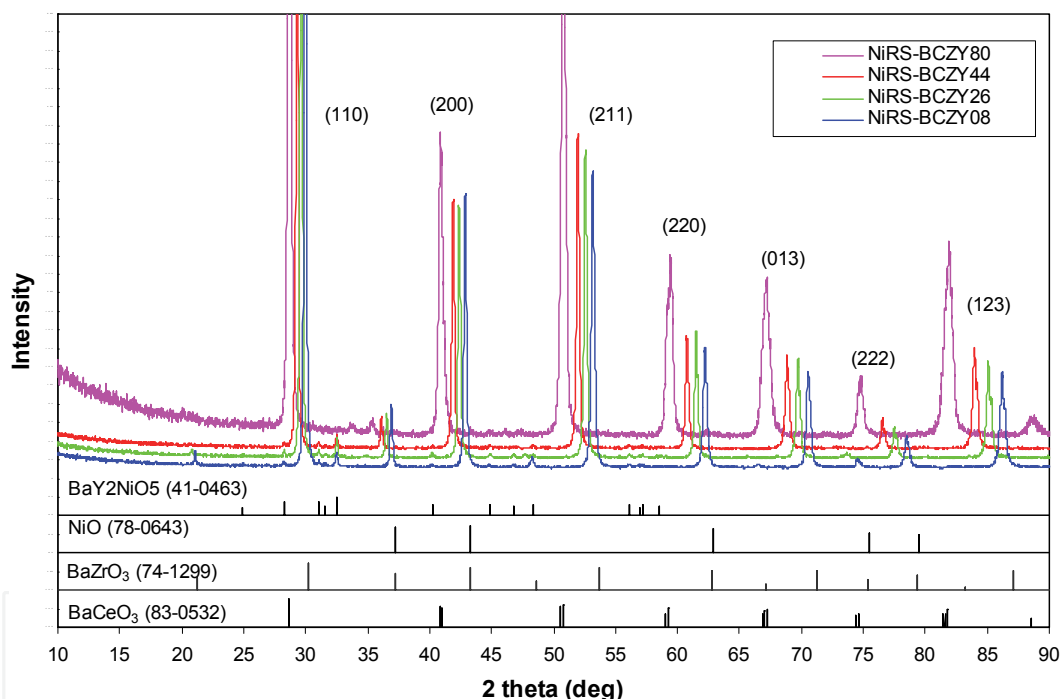
Fig. 2. XRD patterns for 1wt% NiO-reactive sintered BCZY80, BCZY44, BCZY26 and BCZY08 dense ceramics. The major perovskite peaks are shown indexed to the cubic system.

It may be observed that in each set, the major peak in BCZY80 shifts to the corresponding peak in BCZY08 as the Ce/Zr ratio decreases. It may also be seen that the BCZY08 peaks are shifted to the left from the undoped $BaZrO_3$, which is characteristic of the decrease in lattice parameter when Y^{3+} ions substitutes for the larger Zr^{+4} ions on B-sites. The peaks that did not shift were identified as a second phase, BaY_2NiO_5 (41-0463), believed to reside primarily within pores, and possibly also at grain boundaries (Tong, et al. 2010). The pattern for NiO (78-0643) is also included. All of the NiO peaks coincide with $BaZrO_3$ peaks, however, an expanded high index portion of the patterns between 76° and 80° is shown in Figure 3, which indicates the location of the (222) peaks for both NiO and $BaZrO_3$. It may be seen that

there is no evidence for the existence of NiO as a second phase, which would be clearly seen even at the 1 wt% concentration. The highest intensity peaks for the compounds $NiBaO_2$ and $NiBaO_3$ are at 26.26^{o} and 26.06^{o} respectively, and neither is visible in any of the patterns. The conclusion is that most of the original NiO has been incorporated into BaY_2NiO_5. However, the existence of this phase requires excess zirconia and ceria, but no peaks of either of these phases were detected.
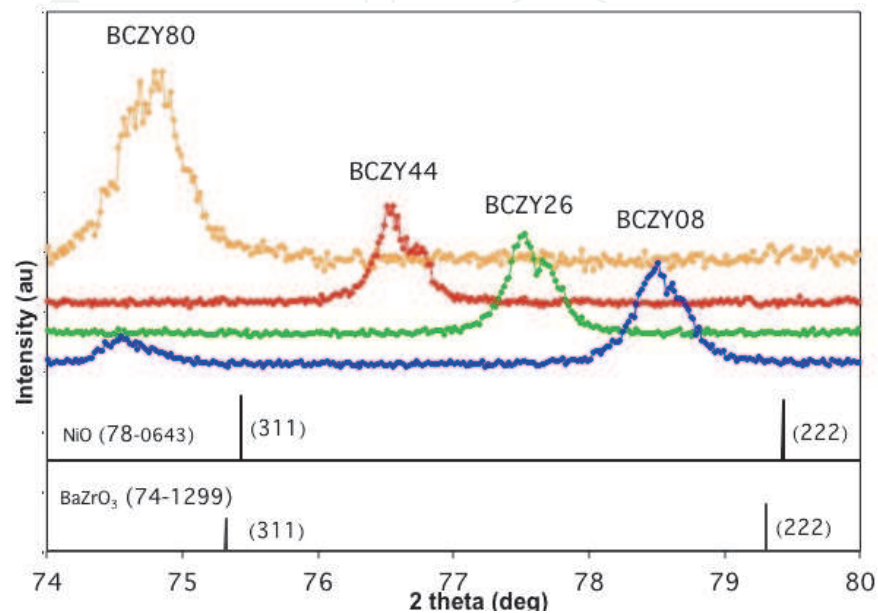
Fig. 3. XRD patterns for 1wt% NiO-reactive sintered BCZY with 20 mol% Y from Fig 1 between 74° and 80°. The (222) peaks are shown for NiO and $BaZrO_3$. The corresponding (222) peaks for the BCZY series are shifted to smaller angles (decreasing lattice parameter).
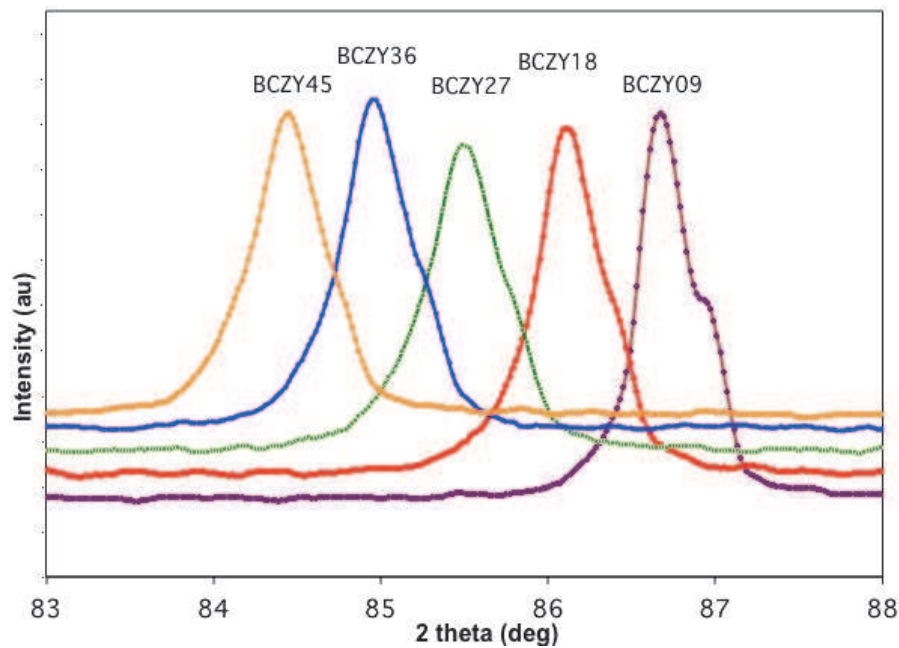
Fig. 4. Set of (123) XRD peaks for 1wt% NiO-BCZY with 10 mol% Y showing uniform spacing. (Shoulders are due to Cu K-β radiation.)

It is also seen in Figure 3 that the peaks are evenly spaced across the whole range of the solid solution for the 20 Mol% Y series. This effect is even more striking in Figure 4 for the 10 mol%Y BCZY series where the highest-index (123) peaks are shown. The shoulders slightly to the right of the central peaks are due to Cu K-β radiation.

The pseudocubic lattice parameters are given in Table 3 along with the other bulk properties derived from the lattice constant. The end members of the solid solution, $BaZrO_3$ and $BaCeO_3$ are listed first, followed by the set of 20 mol% and then 10 mol% Y BCZY specimens.

Ceramic Material	Pseudocubic Lattice Param. (A)	Theoretical Density (g/cm³)	Formula Wt. (g/mol)	Mol.Vol. (cm³/mol)
$BaZrO_3$ (74-1299)	4.1816	6.279	276.55	44.041
$BaCeO_3$ (83-0532)	4.4073	6.316	325.45	51.528
BCZ(20 mol%Y)				
1NiBCZY08	4.2110	6.103	274.49	44.974
1NiBCZY26	4.2547	6.128	284.27	46.391
1NiBCZY44	4.3051	6.118	294.05	48.059
1NiBCZY80	4.3959	6.245	319.52	51.164
BCZ(10 mol%Y)				
1NiBCZY09	4.1970	6.188	275.52	44.528
1NiBCZY18	4.2212	6.190	280.41	45.304
1NiBCZY27	4.2461	6.188	285.30	46.108
1NiBCZY36	4.2674	6.200	290.19	46.806
1NiBCZY45	4.2881	6.214	295.08	47.490

Table 3. Pseudocubic lattice parameters for 1wt% NiO-reactive sintered BCZY. The major perovskite peaks are indexed to the cubic system. Theoretical density, formula molecular weight and molar volume are based on the lattice parameters derived from fitting XRD data.

The XRD peaks in Figures 3 and 4 clearly show that a complete BCZY solid solution has been achieved by reactive sintering. No mixed phases are present, and all the data is well indexed to the cubic system. The lattice parameters from Table 3 have been plotted in Figure 5 versus the ratio of B-sites occupied by cerium to the occupation by either cerium or zirconium. It may be observed that a linear relationship exists from which the unit cell volume may be estimated,

$$\bar{a} = 0.194 \frac{[Ce]}{[Ce]+[Zr]} + 4.204 \tag{2}$$

where $\bar{a}$ is in Å, and the pseudocubic unit cell volume, $V_c = \bar{a}^3$. The lattice parameters for undoped $BaCeO_3$ (83-0532) and $BaZrO_3$ (74-1299) are 4.4073Å and 4.1816Å, respectively. The corresponding extrapolations using our linear fit are 4.398Å and 4.204Å. The regression underestimates the lattice constant for $BaCeO_3$ while over estimating it for $BaZrO_3$, but the discrepancy is less than 1%, suggesting that the change in lattice parameter resulting from substitution of 10-20 mol% yttrium on B-sites is relatively small compared with the

Co-Ionic Conduction in Protonic Ceramics of the
Solid Solution,BaCe$_{(x)}$Zr$_{(y-x)}$Y$_{(1-y)}$O$_{3-\delta}$ Part I: Fabrication and Microstructure

489

difference resulting from zirconium and cerium, alone. Also plotted are several published values from the literature. The striking feature is that all barium cerate-zirconate solid solutions exhibit almost the same linear behavior, independent of dopant type, dopant concentration or sintering additive used. The slopes are about the same in all cases, and only BCZNd (Ryu & Haile, 1999) exhibits a slightly smaller overall lattice constant than all the specimens doped with gadolinium or yttrium.

$$y = 0.1938x + 4.2036$$
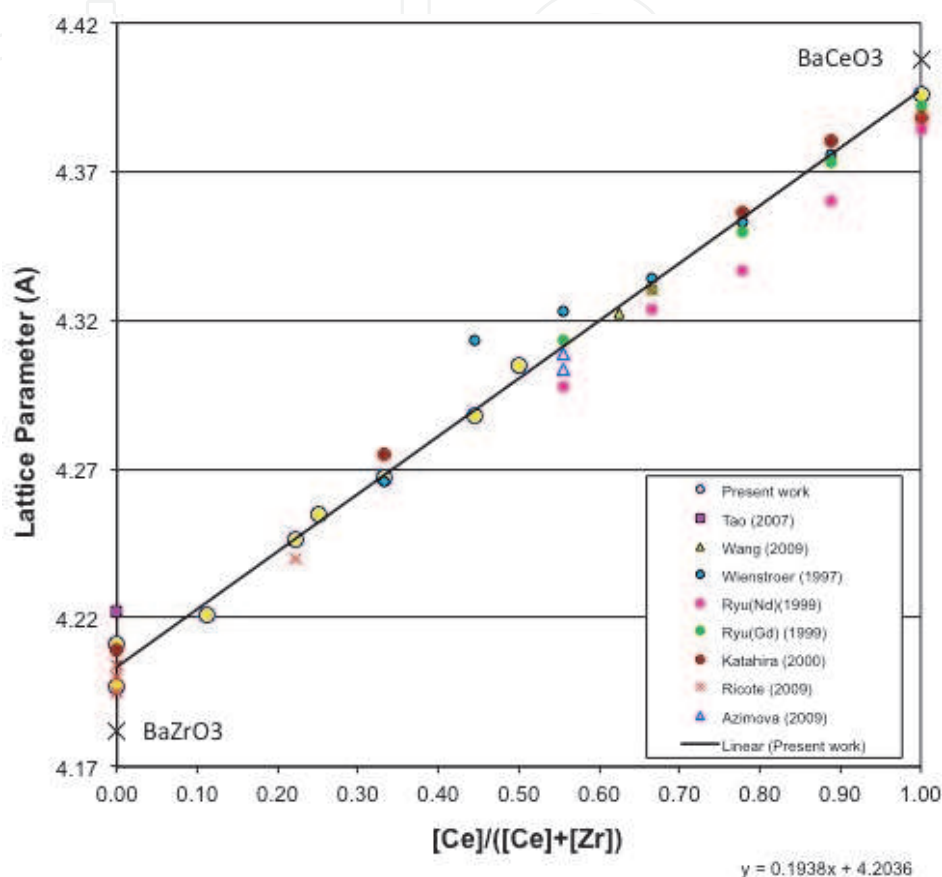
Fig. 5. Pseudocubic lattice parameters vs. the ratio of occupied B-sites Ce^{+4}/(Ce^{+4}+Zr^{+4}). The slopes are invariant to dopant, dopant concentration or MOx sintering additive.

5.2 As-fired NiRS-BCZY26 microstructure
For the further study, the compositions *n/m* = 1/3 (BCZY26) and 2/7 (BCZY27) were selected. These specimens were prepared from extruded tubes 6mm OD x 4.5mm ID. A SEM image of an as-fired NiRS-BCZY26 polished and thermally etched at 1425 °C for 35 minutes is shown if Figure 6. The ceramic is well-sintered with average grain size of 2 to 5 microns. Figure 7 shows a micrograph of an attempt to reactive sinter BCZY without NiO addition. The precursor powders have barely reacted at all and practically no sintering has taken place. This underscores the dramatic effect brought about by a small addition of NiO.

A specimen prepared by focused ion beam (FIB) etching and removal from a bulk ceramic is shown in bright field TEM in Figure 8. It is clear by the 120° dihedral angles at triple points and absence of pores that sintering is complete. The investigation concluded that most of the grain boundaries were clean, but evidence of some amorphous grain boundaries was observed. A high resolution TEM is shown in Figure 9 showing a clean grain boundary
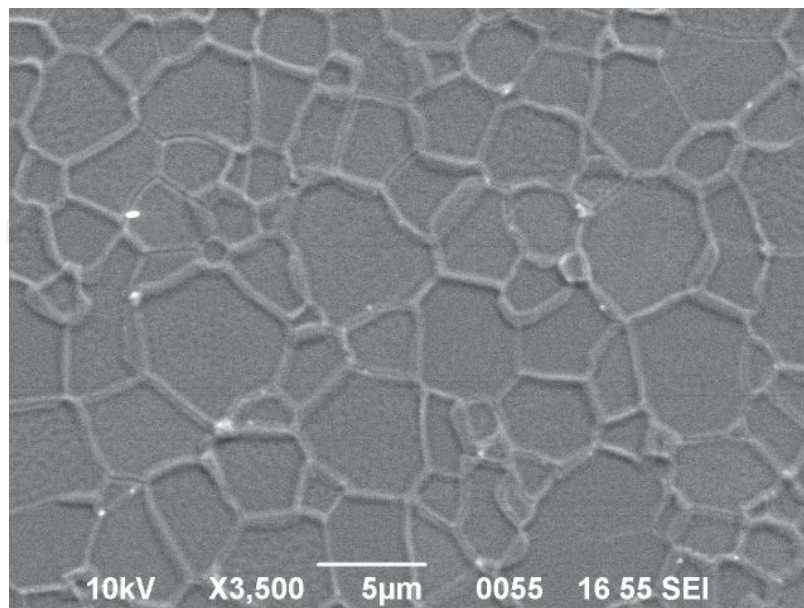
Fig. 6. As-fired polished and thermally etched (1425 °C, 35 min.) surface of 1wt% NiO-reactive sintered BCZY26 (3500x).
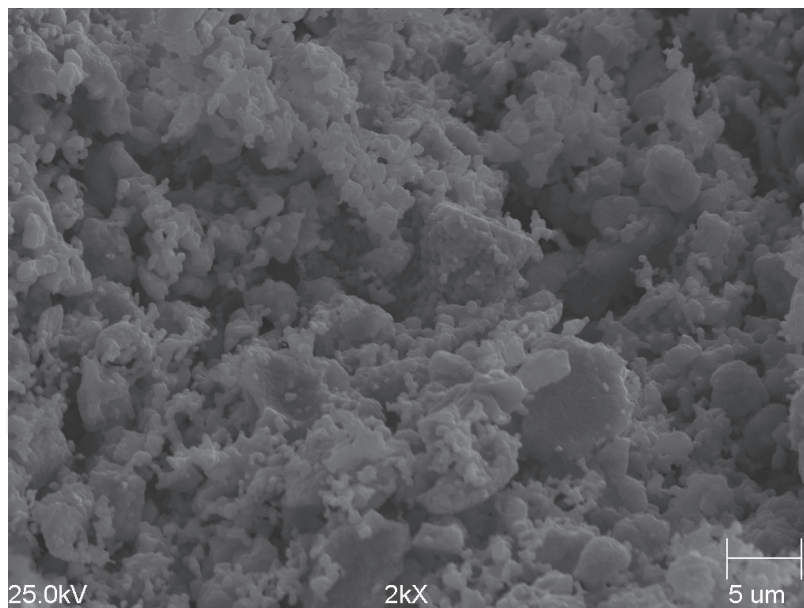

Fig. 7. Micrograph of attempt to reactive sintered BCZY26 without NiO addition (2000x).

intersecting with two amorphous ones at a triple point. This is obviously a significant finding, since high grain boundary impedance has long been suspected as the reason why the proton conductivity of doped barium zirconate is lower than expected. If a continuous network of amorphous grain boundaries were to form during sintering, these could well be blocking to proton transport on a macroscopic scale. The nature and extent of these amorphous grain boundaries is currently receiving a great deal of attention.

Co-Ionic Conduction in Protonic Ceramics of the
Solid Solution, $BaCe_{(x)}Zr_{(y-x)}Y_{(1-y)}O_{3-\delta}$ Part I: Fabrication and Microstructure
491
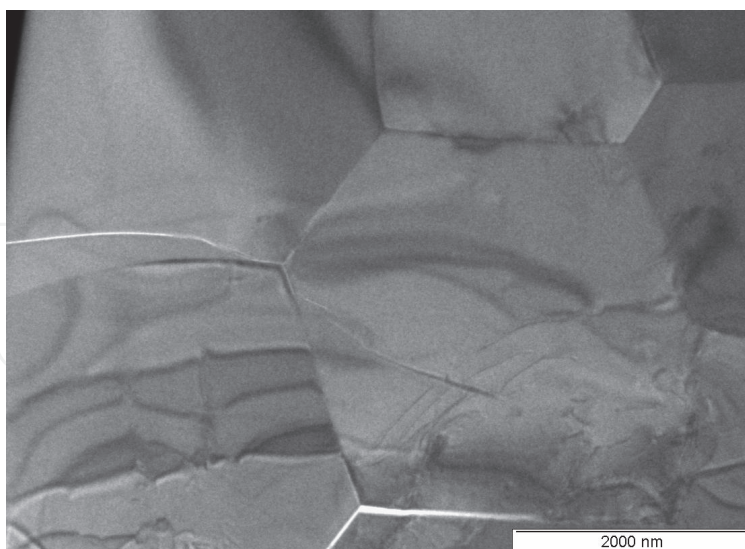
Fig. 8. Bright field TEM of reactive sintered BCZY26. The fracture at lower grain boundaries is the result of mechanical sectioning of specimen.
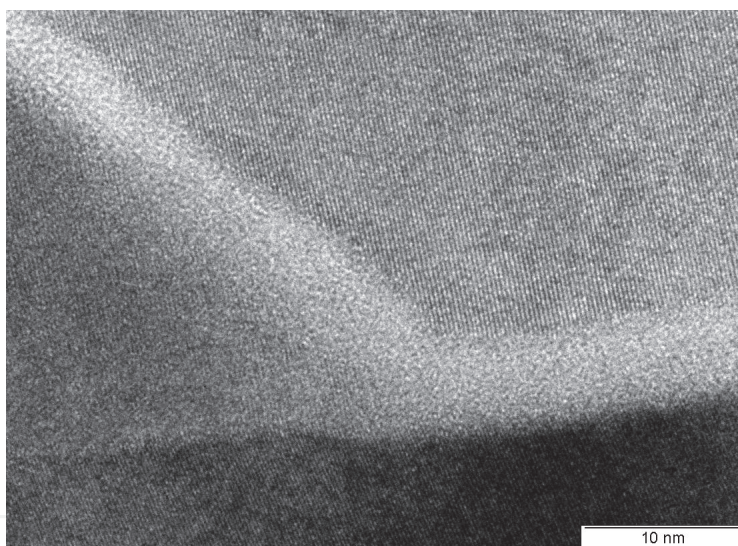

Fig. 9. HR TEM of reactive sintered BCZY26. The image shows that some of the grain boundaries are amorphous .

5.3 Solid state reactive sintering

Pure barium zirconate $BaZrO_3$ and barium cerate $BaCeO_3$ powders are relatively easy to fabricate by solid state reaction, but the incorporation of the large, aliovalent yttrium ions into the lattice is necessary in order to create the oxygen vacancies required for ion transport. In earlier experiments at CoorsTek in Golden, attempts to synthesize phase-pure BZY10 (10 mol% yttria-doped barium zirconate ($BaZr_{0.9}Y_{0.1}O_{3-d}$)) by solid-state reaction of ZrO_2, Y_2O_3 and $BaCO_3$ powders were not successful at temperatures as low as 1550 °C. Only recently was it discovered that very phase-pure BZY10 (BCZY09) calcine powder could be produced with the addition of a small amount of NiO. This was suggested by the analogy to the experience gained in fabricating NiO reactive sintered yttria stabilized zirconia

(NiYRSZ) (Swartzlander & Coors, 2009). However, when binders were added and the pre-calcined powder was compacted and sintered at 1550 °C, the resulting ceramic specimens were porous, with a fired density of only 60-70%. Subsequent experiments demonstrated that dense BZY10 could be fabricated by eliminating the traditional calcining step altogether. By mixing and compacting just the precursor powders of zirconia, yttria, barium carbonate, and a small amount of NiO, dense, phase-pure BZY10 could be fabricated with relative ease at only 1550 °C. This has become the process we refer to as NiO reactive sintered BCZY. A variant process was attempted to make BZY10 from pre-calcined 10 mol% yttria-stabilized zirconia (Tosoh 10YS), barium carbonate plus some NiO, but this led to sintering difficulties and considerable residual YSZ phase in the resulting ceramic. Apparently it is necessary to simultaneously create the cubic barium zirconate phase, incorporate the yttria dopant, and obtain the well-sintered grain boundaries during sintering in order to fabricate this ceramic. Ironically, this simple process uses very inexpensive raw materials, costing no more than about $5-10 per kilogram, and readily accessible air-fire sintering temperatures, making the commercialization of this important material very straightforward.

Clearly, reactive sintering involves several complicated steps. We hypothesize the following: Upon decomposition of $BaCO_3$, the reaction of BaO and NiO, beginning about 1100 °C, produces a liquid phase that enhances the transport along grain boundaries of all the cations involved in the solid state reactions. As temperature increases, $BaCe_xZr_{(1-x)}O_3$ begins to form, making the BaO-NiO melt increasingly nickel oxide rich and raising the melting temperature. Initially, $BaCe_xZr_{(1-x)}O_3$ has only a small concentration of intrinsic oxygen vacancies. Incorporation of some percentage of aliovalent dopants on B-sites lowers the Gibbs free energy, but without oxygen vacancies, diffusion by relatively large acceptor dopant ions like yttrium is difficult. In the case of BCZY, the yttrium ions must substitute on B-sites in the perovskite lattice by first diffusing into the zirconia or ceria grains. Since small cations, such as Ni^{2+} (0.69Å), are much more facile than Y^{3+} (0.92Å), the defect reaction initially takes place with the smaller, Ni^{2+} dopant ions, which can easily diffuse into the grain by substituting on B-sites. However, diffusion of Ni^{2+} into the grain requires extra charge compensation by creating oxygen vacancies on the anion sublattice (although more complex defect reactions involving electron holes are certainly possible). As the concentration of oxygen vacancies increases, diffusion of the larger Y^{3+} ion is facilitated by the vacancy transport mechanism. The nickel ions are too small to stabilize the perovskite structure by occupying the space of a B-site Ce^{4+} (0.94Å) or Zr^{4+} (0.79Å) and the requirement for charge compensation too great. The perovskite structure is more stable with the closer matched yttrium than nickel on B-sites, so nickel ions will ultimately be displaced by yttrium above a certain threshold concentration. This ion exchange mechanism occurs simultaneously throughout the entire body matrix promoting phase equilibria within grains and at grain boundaries during sintering. Ultimately, as the equilibrium BCZY phase forms, the nickel ions are exsolved and precipitated once again at grain boundaries as NiO or BaY_2NiO_5. The reason that reactive sintering does not work with pre-calcined YSZ powder is because it is already a stable phase that has no tendency to convert from the flourite phase to the perovskite phase at the low reactive sintering temperature, and nickel ions have no role to play in the required solid state ion exchange reactions. Similarly, precalcined BCZY powder does not densify even when NiO is added, which demonstrates that reactive sintering involves much more than just conventional liquid phase sintering. The kinetics of

Co-Ionic Conduction in Protonic Ceramics of the
Solid Solution, $BaCe_{(x)}Zr_{(y-x)}Y_{(1-y)}O_{3-\delta}$ Part I: Fabrication and Microstructure

493

reactive sintering involves the coordination of liquid phase sintering for grain boundary formation and ion exchange for bulk BCZY phase formation.

5.4 Microstructure after reduction

Conductivity testing of BCZY requires extended operation in moist and dry hydrogen at elevated temperatures. Post-reduction microstructure analysis was conducted to determine if the residual NiO causes any deleterious effects. Figure 10 shows a FESEM fracture surface of BCZY26 after multiple temperature cycles between 200 and 1000 °C in moist and dry 5% H_2/bal Argon. It may be observed in the image that nearly all of the fracture has occurred at grain boundaries, unlike the as-fired ceramic that exhibited mostly transgranular fracture. This suggests a weakening of the structure at grain boundaries due to a combination of reducing atmosphere and strain from temperature excursions. Also visible in the micrograph is a network of microcracks. The ceramic specimens typically failed catastrophically upon decreasing temperature in moist hydrogen or argon at some point below about 400 °C. In dry atmosphere, no fracture was observed. We believe the fracture is due to the strain induced by water of hydration at elevated temperatures that remains "frozen-in" at low temperatures from stoichiometric expansion. We have demonstrated with BCY and BZY that lattice hydration causes a measureable length dilation that has actually been used in TCE measurements to determine the extent of hydration (Coors & Swartzlander, 2005). Apparently, in the case of reactive sintered BCZY, the stress exceeds the strength of the material. This obviously is a matter of concern that will require careful management of operating parameters. Recently, preliminary investigations have indicated that much stronger and durable ceramic results when $BaSO_4$ is substituted for $BaCO_3$. In this case the sintering temperature is higher (~1600 °C) because of the higher decomposition temperature of the sulfate, but distinctly improved grain boundaries are obtained. Also, reduction of the yttrium dopant concentration from 20 to 10 mol% seems to improve the mechanical properties without
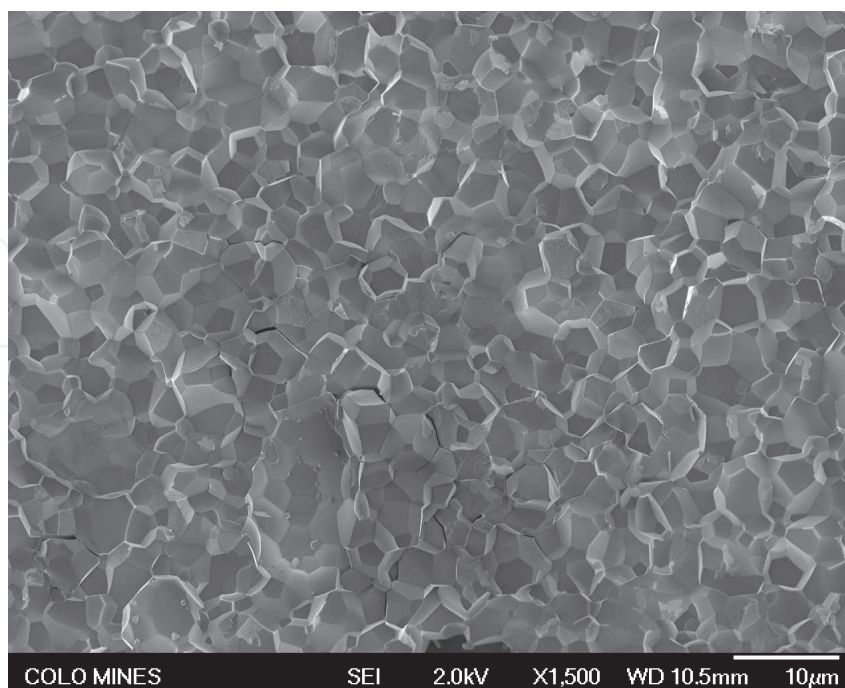

Fig. 10. FESEM Micrograph reduced BCZY26 fracture surface (1500x).

much sacrifice in conductivity, even though the oxygen vacancy concentration is one half as much. The formulation that seems to provide the best compromise of chemical stability, mechanical strength and proton conductivity is 1NiBCZY27.

Figure 11 is an enlarged view of a residual pore in 1NiBCZY26 after reduction. In this case, the surfaces of the grains are as-fired. The fracture is clearly visible along some grain boundaries. The most interesting feature of the micrograph is the presence of nanoprecipitates occurring predominantly along grain boundaries. Figure 12 is an EDS scan of one of these compared to the bulk grain. The precipitates were found to be mostly nickel.
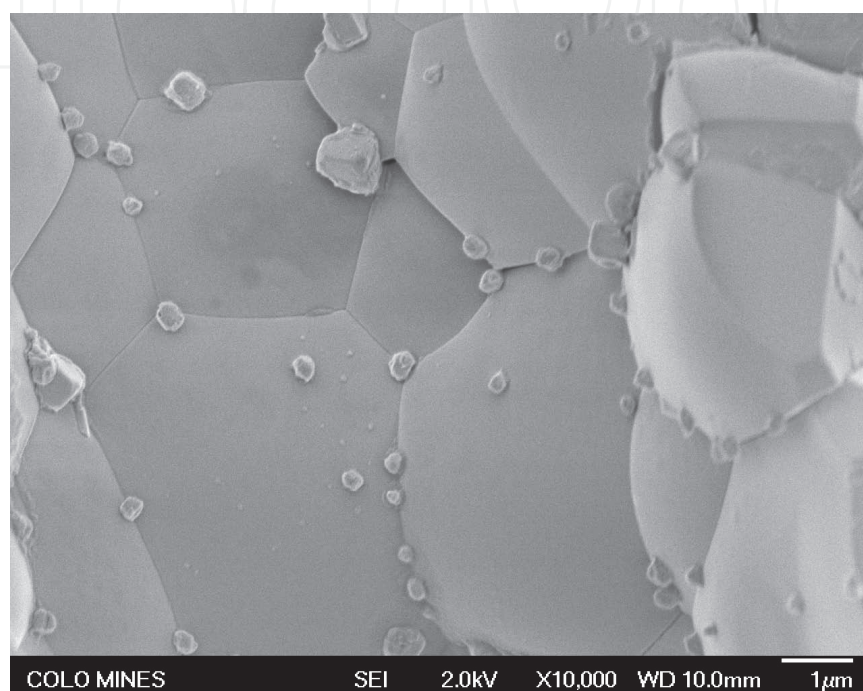
Fig. 11. FESEM Micrograph reduced BCZY26 surface of internal void with metallic Ni precipitates (10000x).

The specimen was subsequently analyzed for magnetic properties to determine the nature of the nickel precipitates using a Quantum Design PPMS. Figure 13 (top) shows the magnetic moment versus temperature. The sharp drop at 620K, the Currie temperature for bulk nickel, is the signature for metallic nickel. In Figure 13 (bottom), the magnetic moment versus field strength, H, is shown. The black curve is for a piece of nickel wire calibrated to the same nickel mass as in the 1NiBCZY26 specimen. The red curve is for the fully reduced BCZY26 specimen. It may be seen that the magnetic saturation is characteristic of ferromagnetic bulk metallic nickel. Also, the shallow slope of the magnetization curve at low field is characteristic of small, isolated nickel particles, which is consistent with the small precipitates in Figure 11. Even at 1000 Gauss, the magnetization has reached less than half its saturation value, in sharp contrast to the curve for the bulk nickel wire, which was almost fully saturated at this same field. It was possible to determine quantitatively from the saturated magnetization at 5000 Gauss that the wt% of metallic nickel in the specimen was 0.854%. A subsequent measurement using a QD-SQUID gave a value of 0.882%. The actual value for the 1NiBCZY26 specimen determined by X-ray Fluorescence was 0.825%. Within experimental error, virtually 100% of the original NiO has been reduced to bulk Ni metal. It

Co-Ionic Conduction in Protonic Ceramics of the
Solid Solution,BaCe$_{(x)}$Zr$_{(y-x)}$Y$_{(1-y)}$O$_{3-\delta}$ Part I: Fabrication and Microstructure
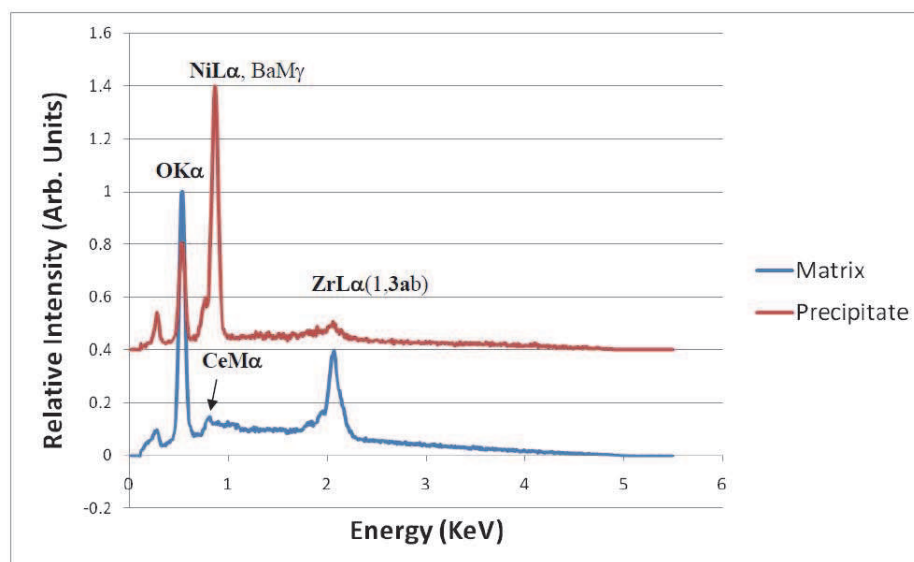
495

Fig. 12. EDS acquired using an electron beam with 5 KeV of energy. Ce and Ba have weak M band excitations (strong L bands for both occur at ~4 KeV). Nickel present predominantly in the nanoprecipitate.

is possible to draw two important conclusions from this finding: 1) very little, if any, nickel was lost during sintering and subsequent elevated temperature operation, and 2) a negligible fraction of the original nickel remains in the ceramic as ions. Although it is not possible to rule out that some Ni nanoprecipitates may exist within grains, as was found to be the case with Ni-reactive sintered yttria-stabilized zirconia (Coors, et al. 2009). The SEM image in Figure 11 suggest that most occur at grain boundaries. In any event, the possibility of nickel residing intersticially or substitutionally on regular lattice sites as ions may be considered remote.

XRD patterns were obtained on 1NiBCZY26 after reduction. The as-fired and post reduction patterns are shown in Fig. 14. There was no change in lattice parameter, and the strongest metallic nickel line (111) at 44.5° is just barely visible. The lower figure expands the region from 28° to 33° in which the four strongest peaks of the phase, BaY$_2$NiO$_5$ (00-041-0463) occur. These peaks are clearly visible in the as-fired ceramic, but have completely disappeared in the reduced specimen. The phase was identified as a grain boundary phase left over from SSRS (Tong, et al. 2010). With some of the barium tied up in this grain boundary phase, it is expected that the as-fired perovskite is slightly A-site deficient, but upon reduction, metallic nickel nanoprecipitates form, and the barium and yttrium are apparently dissolved back into the perovskite lattice. For most commercial applications envisioned with these protonic ceramics, reducing atmosphere is anticipated. This will certainly be the case for hydrogen separation and membrane reactors. In the case of PCFCs, the ceramic will be exposed to reducing atmosphere on one side and oxidizing on the other. For steam permeable membranes, SPMs, intermediate oxygen partial pressures may be encountered which are not low enough to reduce the barium-yttrium nickelate phase. It has yet to be determined if the reduction of this grain boundary phase is reversible or to what extent proton transport across grain boundaries may be influenced by this phenomenon.
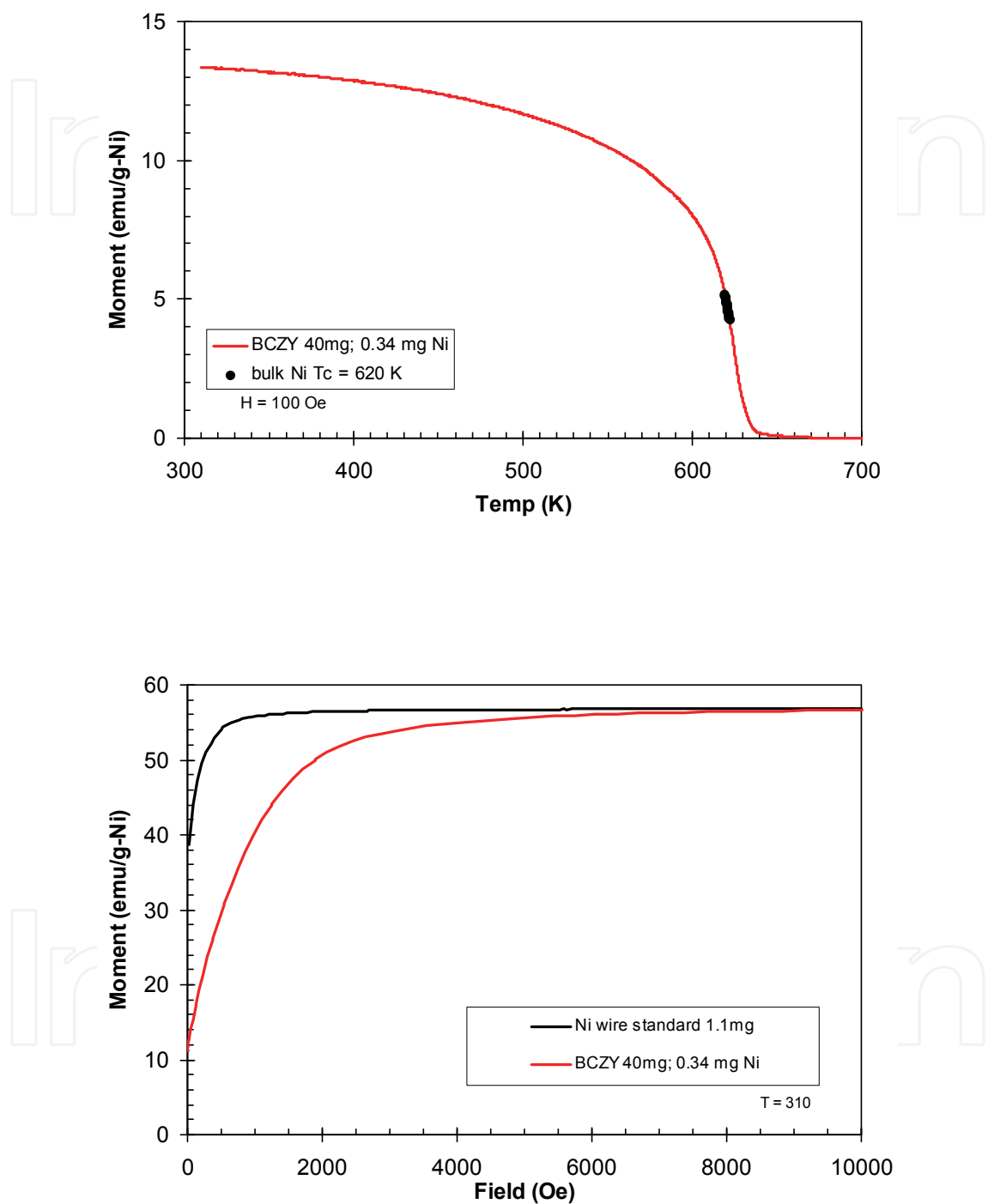
Fig. 13. Reduced NiRS-BCZY26 (top) magnetic moment vs. temperature at fixed field 100 Oe and (bottom) vs. field at fixed temperature (310 K) by QD-PPMS.

Co-Ionic Conduction in Protonic Ceramics of the
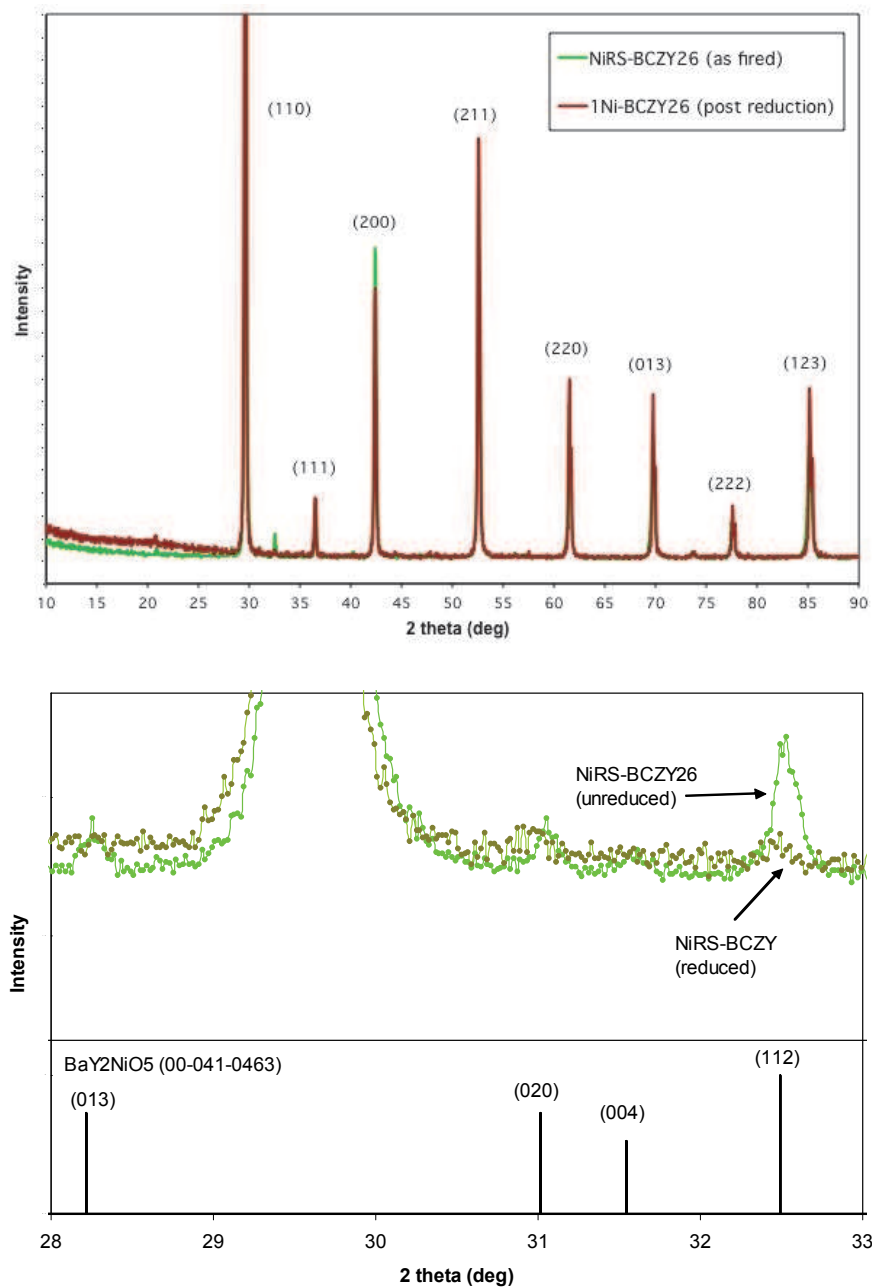Solid Solution,$BaCe_{(x)}Zr_{(y-x)}Y_{(1-y)}O_{3-\delta}$ Part I: Fabrication and Microstructure

497

Fig. 14. NiRS-BCZY26 XRD as-fired (light green) and after reduction (dark green) Top figure 10-90° 2 θ and lower pattern 28-33° with four strongest peaks of BaY_2NiO_5 (00-041-0463) pattern.

6. Conclusions

Several compositions of the solid solution $BaCe_xZr_{0.8-x}Y_{0.2}O_{3-d}$ (0≤x≤0.8) were prepared by solid state reactive sintering SSRS using 1 wt% NiO as a sintering additive. Dense, phase-pure ceramics were obtained with NiO while practically no solid-state reaction or sintering took place without NiO. It was found that a complete solid solution existed over the entire composition range, and it was observed that a linear relationship existed between the pseudocubic lattice constant and the ratio of ceria to ceria plus zirconia on B-sites:

a(Å)=0.194*[Ce]/([Ce]+[Zr])+4.204). A relatively weaker dependency of lattice constant on dopant ion was observed. XRD of as-fired ceramics exhibited BaY_2NiO_5 as the only identifiable second phase in the, otherwise, phase-pure perovskites. Thought to be a grain boundary phase, BaY_2NiO_3 was found to be reduced completely to metallic nickel precipitates that decorated grain boundaries after extended processing in moist and dry hydrogen at high temperatures. The mechanical strength of as-fired ceramic was excellent, while the strength of reduced material was considerably lower – a condition that warrants caution. Stoichiometric expansion due to frozen in hydration causes ceramic failure at low temperatures. However, substitution of $BaSO_4$ for $BaCO_3$ in the starting powders and reduction of yttria dopant concentration seem to hold promise as a solution to this problem. Further evaluation the grain boundary integrity is necessary as these materials are being considered for practical applications. It may be necessary to add other components to compensate for loss of strength at grain boundaries. NiO solid state reactive sintering was demonstrated to be a remarkably easy and inexpensive way to fabricate this potentially important class of protonic perovskites.

7. Acknowledgments

8. References

Azimova, M. & McIntosh, S. (2009). Transport properties and stability of cobalt doped proton conducting oxides. *Solid State Ionics,* Vol.180[2-3], pp.160-167

Babilo, P. & Haile, S.M. (2005). Enhanced sintering of yttrium-doped barium zirconate by addition of ZnO. *J. Am. Ceram. Soc.*, Vol.88, No.9, pp.2362-2368

Coors W.G. & Swartzlander, R. (2005). Partial conductivity measurements in $BaCe_{0.9}Y_{0.1}O_{3-d}$ by impedance spectroscopy. *Proceedings of the 26th Risø International Symposium on Materials Science: Solid State Electrochemistry*, Linderoth, et al., Eds., September 4-8, pp.185-196

Coors, W.G.; Zhao, F.; Heck, B. (April 2008). Reaction sintered BCY10 ceramic – Fabrication and microstructure," Internal CoorsTek Report (available from author upon request)

Coors, W.G. (Sept 2008). Reaction sintered BZY10 ceramic - Fabrication and microstructure, Internal CoorsTek Report, (available from author upon request)

Coors, W.G.; O'Brien, J.; & White, J. (2009). Conductivity degradation of NiO-containing 8YSZ and 10YSZ electrolyte during reduction. *Solid State Ionics,* Vol.180, pp.246-251

Costa, R.; Grünbaum, N.; Berger, M.-H.; Dessemond, L.; Thorel, A. (2009). On the use of NiO as sintering additive for $BaCe_{0.9}Y_{0.1}O_{3-a}$. *Solid State Ionics,* Vol.180, pp.891-895

Galasso, F.S. (1969) *Structure, Properties and Preparation of Perovskite-type Compounds*, Pergamon Press, Ltd.,

Guo, Y.; Lin, Y.; Ran, R.; Shao, Z. (2009). Zirconium doping effect on the performance of proton-conducting $BaZr_yCe_{(0.8-y)}$ $Y_{0.2}O_{3-\square}$ (0.0≤y≤0.8) for fuel cell applications. *J. Power Sources*, Vol.193, pp.400-407

Irvine, J; Tao, S.; Savaniu, C.; & Kruth, A. (2007). Steam Electrolysis, US Patent Application 2007/0278092, Dec. 6, 2007

Iwahara, H.; Uchida, H.; Ono, K.; & Ogaki, K. (February 1988). Proton conduction in sintered oxides based on $BaCeO_3$. *J. Electrochem. Soc.: Solid State Science and Technology*, pp.529-533

Katahira, K.; Kohchi, Y.; Shimura, T.; & Iwahara, H. (2000). Protonic conduction in Zr-substituted $BaCeO_3$. *Solid State Ionics*, Vol.138, pp.91-98

Kingery, W.D.; Bowen, H.K.; & Uhlmann, D.R. (1960) *Introduction to Ceramics*, (2nd Ed.), John Wiley & Sons, ISBN 0-471-47860-1, p.448

Kreuer, K.-D. (1999). Aspects of the formation and mobility of protonic charge carriers and the stability of perovskite-type oxides. *Solid State Ionics*, Vol.125, pp.285-302

Kreuer, K.-D. (2003). Proton-conducting oxides. *Annu. Rev. Mater. Rev.,* Vol.33, pp.333-359

Magrez, A. & Schober, T. (2004). Preparation, sintering, and water incorporation of proton conducting $Ba_{0.99}Zr_{0.8}Y_{0.2}O_{3-\square}$, *Solid State Ionics*, Vol.175, pp.585-588

Munch, W.; Kreuer, K.-D.; Seifert, G.; & Maier, J. (2000). Proton diffusion in perovskites: Comparison between $BaCeO_3$, $BaZrO_3$, $SrTiO_3$, and $CaTiO_3$ using quantum molecular dynamics. *Solid State Ionics*, Vol.136-137, pp.183-189

Ryu, K. & Haile, S. (1999). Chemical stability and proton conductivity of doped $BaCeO_3$ – $BaZrO_3$ solid solutions. *Solid State Ionics*, Vol.125, pp.355-367

Ricote, S.; Bonanos, N.; Marco de Lucas, M.C.; Caboche, G. (2009). Structural and conductivity Study of the proton conductor $BaCe_{(0.9-x)}Zr_xY_{0.1}O_{3-\square}$ at intermediate temperatures. *J. Power Sources,* Vol.193, pp.189-193

Ricote, S.; Bonanos, N.; Caboche, G. (2009). Water vapour solubility and conductivity study of the proton conductor $BaCe_{(0.9-x)}Zr_xY_{0.1}O_{3-\square}$, *Solid State Ionics,* Vol.180, pp.990-997

Ricote, S.; Bonanos, N.; Wang, H.J.; Haugsrud, R. (2011). Conductivity, transport number measurements and hydration thermodynamics of $BaCe_{0.2}Zr_{0.7}Y_{(0.1-x)}Ni_xO_{(3-d)}$. *Solid State Ionics,* Vol.185, pp.11-17

Schober, T. & Bohn, H. (2000). Water vapor solubility and electrochemical characterization of the high temperature proton conductor $BaZr_{0.9}Y_{0.1}O_{2.95}$. *Solid State Ionics*, Vol.127, pp.351-360

Schober, T. (2005). Transformation of an oxygen ion conductor to a proton conductor by solid state reaction. *Solid State Ionics*, Vol.176, pp.2275-2277

Shimura, T.; Tanaka, H.; Matsumoto, H.; & Yogo, T. (2005). Influence of the transition-metal doping on conductivity of a $BaCeO_3$-based proton conductor. *Solid State Ionics* Vol.176, pp.2945-2950

Swartzlander, R. & Coors, W.G. (2009). Preparation of yttria-stabilized zirconia reaction sintered products. US Patent 7,527,761, May 5, 2009

Tao, S. & Irvine, J. (2006). A stable, easily sintered proton-conducting oxide electrolyte for moderate-temperature fuel cells and electrolyzers. *Advanced Materials*, Vol.18, pp.1581-1584

Tao, S. & Irvine, J. (2007). Conductivity studies of dense yttrium-doped $BaZrO_3$ sintered at 1325 °C. *J. Solid State Chem.*, Vol.180, pp.3493-3503

Tong, J.; Clark, D.; Bernau, L.; Subramaniyan, A. & O'Hayre, R. (2010). Proton-conducting yttrum-doped barium cerate ceramics synthesized by a cost-effective solid-state reactive sintering method. *Solid State Ionics*, Vol.181, pp.1486-1498

Tong, J.; Clark, D.; Hoban, M.; & O'Hayre, R. (2010). Cost-effective solid-state reactive sintering method for high conductivity proton conducting yttrium-doped barium zirconium ceramics. *Solid State Ionics*, Vol.181, pp.496-503

Tong, J.; Clark, D.; Bernau, L.; Sanders, M.; & O'Hayre, R. (2010). Solid-state reactive sintering mechanism for large-grained yttrium-doped barium zirconate proton conductiving ceramics. *J. Mater. Chem.*, Vol.20, pp.6333-6341

Wang, H.; Peng, R.; Wu, X.; Hu, J.; & Xia, C. (2009). Sintering behavior and conductivity of yttrium-doped $BaCeO_3$-$BaZrO_3$ solid solutions using ZnO additives. *J. Am. Ceram. Soc.*, Vol.92, No.11, pp.2623-2629

Wienströer, S. & Wiemhöfer, H.-D. (1997). Investigation of the influence of zirconium substitution on the properties of neodymium-doped barium cerates. *Solid State Ionics*, Vol.101-103, pp.1113-1117

Xu, X.; Tao, S.; & Irvine, J. (2010). Proton conductivity of potassium doped barium zirconates. *J. Solid State Chem.*, Vol.183, pp.93-98

Yamazaki, Y.; Hernandez-Sanchez, R.; Haile, S. (2009). High total proton conductivity in large-grained yttrium-doped barium zirconate. *Chem. Mater.*, Vol.21, pp.2755-2762

Zhong, Z. (2007). Stability and conductivity of the $BaCe_{0.9-x}Zr_xY_{0.1}O_{2.95}$ systems. *Solid State Ionics*, Vol.178, pp.213-230
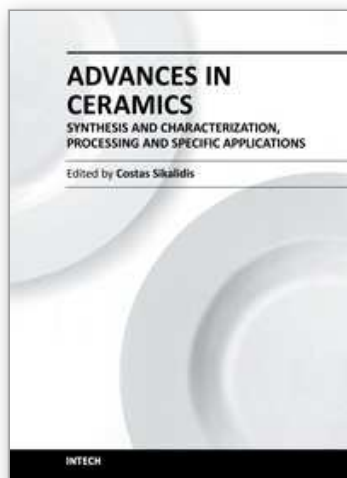
Advances in Ceramics - Synthesis and Characterization, Processing and Specific Applications

Edited by Prof. Costas Sikalidis

ISBN 978-953-307-505-1

Hard cover, 520 pages

Publisher InTech

Published online 09, August, 2011

Published in print edition August, 2011

The current book contains twenty-two chapters and is divided into three sections. Section I consists of nine chapters which discuss synthesis through innovative as well as modified conventional techniques of certain advanced ceramics (e.g. target materials, high strength porous ceramics, optical and thermo-luminescent ceramics, ceramic powders and fibers) and their characterization using a combination of well known and advanced techniques. Section II is also composed of nine chapters, which are dealing with the aqueous processing of nitride ceramics, the shape and size optimization of ceramic components through design methodologies and manufacturing technologies, the sinterability and properties of ZnNb oxide ceramics, the grinding optimization, the redox behaviour of ceria based and related materials, the alloy reinforcement by ceramic particles addition, the sintering study through dihedral surface angle using AFM and the surface modification and properties induced by a laser beam in pressings of ceramic powders. Section III includes four chapters which are dealing with the deposition of ceramic powders for oxide fuel cells preparation, the perovskite type ceramics for solid fuel cells, the ceramics for laser applications and fabrication and the characterization and modeling of protonic ceramics.

How to reference

In order to correctly reference this scholarly work, feel free to copy and paste the following:

W. Grover Coors (2011). Co-Ionic Conduction in Protonic Ceramics of the Solid Solution, BaCe(x)Zr(y-x)Y(1-y)O3- Part I: Fabrication and Microstructure, Advances in Ceramics - Synthesis and Characterization, Processing and Specific Applications, Prof. Costas Sikalidis (Ed.), ISBN: 978-953-307-505-1, InTech, Available from: http://www.intechopen.com/books/advances-in-ceramics-synthesis-and-characterization-processing-and-specific-applications/co-ionic-conduction-in-protonic-ceramics-of-the-solid-solution-bace-x-zr-y-x-y-1-y-o3-part-i-fabrica

INTECH
open science | open minds